One Building Block, Two Different Nanoporous Self-Assembled Monolayers: A Combined STM and Monte Carlo Study

Jinne Adisoejoso,[†] Kazukuni Tahara,[‡] Shengbin Lei,[§,*] Paweł Szabelski,[⊥,*] Wojciech Rżysko,[∥] Koji Inukai,[‡] Matthew O. Blunt,[†] Yoshito Tobe,[‡,*] and Steven De Feyter[†,*]

[†]Department of Chemistry, Division of Molecular Imaging and Photonics, Laboratory of Photochemistry and Spectroscopy, Katholieke Universiteit Leuven, Celestijnenlaan 200 F, B-3001 Leuven, Belgium, [‡]Division of Frontier Materials Science, Graduate School of Engineering Science, Osaka University, Toyonaka, Osaka 560-8531, Japan, [§]Key Laboratory of Microsystems and Microstructures Manufacturing, Ministry of Education, Harbin Institute of Technology, Harbin, 150080, People's Republic of China, and [⊥]Department of Theoretical Chemistry and [∥]Department for the Modeling of Physico-Chemical Processes, Maria-Curie Skłodowska University, Pl. M.C. Skłodowska, 3, 20-031 Lublin, Poland

ABSTRACT

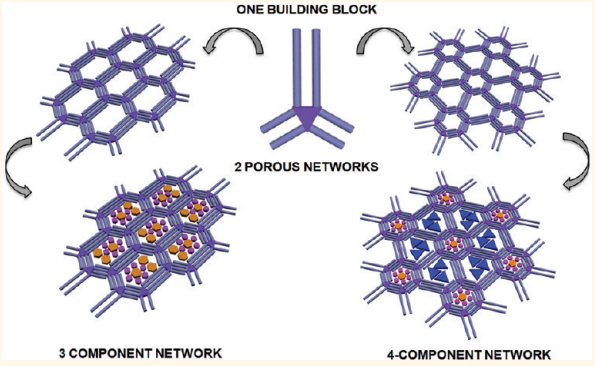

With the use of a single building block, two nanoporous patterns with nearly equal packing density can be formed upon self-assembly at a liquid−solid interface. Moreover, the formation of both of these porous networks can be selectively and homogenously induced by changing external parameters like solvent, concentration, and temperature. Finally, their porous properties are exploited to host up to three different guest molecules in a spatially resolved way.

KEYWORDS: self-assembly · scanning tunneling microscopy · Monte Carlo simulations · phase behavior · multicomponent

Self-assembly of molecules into well-defined supramolecular architectures using noncovalent interactions has a broad application pallet.[1−6] Moreover, so-called surface-confined nanoporous networks are of great interest due to the possibility of using them to immobilize a variety of functional guest molecules in a spatially ordered arrangement.[2,7−12] The formation of nanoporous networks at a liquid−solid interface is favored at low concentration, while nonporous networks with a higher packing density are often formed at higher concentration.[13−18] Apart from concentration, temperature has recently also been explored as a key factor in controlling network formation, by affecting both the kinetics and thermodynamics of the self-assembly process. Increasing the temperature can transform a kinetically trapped network into the thermodynamically favored phase.[19,20] Alternatively, by exploring the experimentally accessible temperature range, several phases can be accessed.[21] Finally, the choice of solvent is also known to greatly influence the network formation at the liquid−solid interface.[22−24] However, predicting the outcome of a self-assembly process for a given molecular building block still remains a challenge, especially when two or more phases are at play.

Among various molecular building blocks, a molecule of symmetry C_{2v} with three intermolecular connection sites is an intriguing case. Through Monte Carlo simulations, we were able to predict the pattern formation of a molecule of symmetry C_{2v} (Figure 1b). Such a molecule, based on the dehydrobenzo[12]annulene motif (DBA1, Figure 1b), was designed and synthesized and its self-assembly behavior was probed at the liquid−solid interface. As predicted, at low concentration, the self-assembly of this molecule leads to two different nanoporous packings which are nearly identical in packing density and differ only in their symmetry, a finding which to the best of our knowledge has not been reported before. By exploring experimental conditions such

* Address correspondence to leisb@hit.edu.cn, szabla@vega.umcs.lublin.pl, tobe@chem.es.osaka-u.ac.jp, steven.defeyter@chem.kuleuven.be.

Received for review November 13, 2011 and accepted December 15, 2011.

Published online December 29, 2011
10.1021/nn204398m

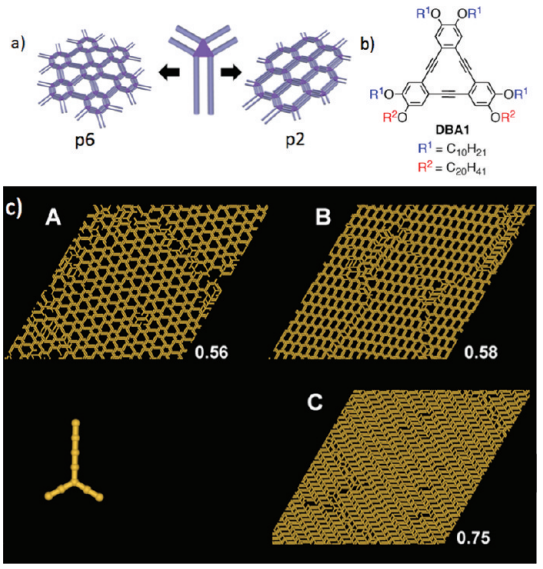

Figure 1. (a) Presentation of the two porous networks which can be obtained using a building block containing four short and two long alkoxy chains. (b) Chemical structure of DBA1. (c) Monte Carlo snapshots of the saturated monolayers formed by molecules of DBA1 (simplified model in the lower left) on a 96 by 96 triangular lattice. Adsorbate density (rounded values), corresponding to an infinite defect-free layer is shown for each pattern. The porous patterns A and B were obtained at $T = 1.5$ and $\mu = -5.5$. The high-density linear pattern C was simulated at $T = 2.0$ and $\mu = 2.0$.

as choice of solvent and solute concentration, we were able to bias the formation of one of the nanoporous phases of equal density. Finally, the functionality of both nanoporous phases for host–guest chemistry is demonstrated.

RESULTS AND DISCUSSION

As reported previously, dehydrobenzo[12]annulenes (DBAs) with six alkoxy chains of equal length self-assemble into two packings at a liquid–solid interface, a close-packed linear one (plane group *p*2) and a nanoporous honeycomb (plane group *p*6) pattern through weak van der Waals interactions arising from interdigitating alkyl chains. Their relative surface coverage depends on the solute concentration.[25−27] Size control of the diameter of the nanowells in the nanoporous pattern was achieved by varying the length of the six identical alkoxy chains ($-OC_{10}H_{21}$ to $-OC_{30}H_{61}$), which form the rims of the pores.[14,28] Moreover, upon deposition of binary mixtures of DBA derivatives with different alkoxy chain lengths, phase separation occurs when the difference in alkyl chain length reaches four methylene groups or more, while mixing and therefore interdigitation between non-equal alkyl chains occurs when the difference is below four methylene groups.[29,30]

Monte Carlo Simulations. We predict that a DBA molecule containing four short and two longer alkoxy chains should lead to networks by recognition of alkyl chains with equal length if the difference in chain length is large enough. Therefore, for a model of C_{2v} molecular building block, a DBA derivative DBA1 with four short decyloxy groups ($OC_{10}H_{21}$) and two longer icosyloxy groups ($OC_{20}H_{41}$) was designed and synthesized (details on synthesis in Supporting Information, section B). Such a difference in alkyl chain length of 10 methylene groups should disable the interdigitation between non-equal alkyl chains. To test this hypothesis, we first used the lattice gas grand cannonical Monte Carlo (GCMC) method with orientational bias sampling which was described in detail elsewhere.[31,32] To simplify the simulations, the structure of DBA1 was modeled consisting of a central segment called core and three linear arms built of 2, 2, and 4 segments, as shown in the lower left part of Figure 1c. Each molecular segment of DBA1 was allowed to occupy one lattice site. The molecules were assumed to interact *via* a short-ranged segment–segment interaction potential limited to nearest neighbors on a triangular grid. The energy of interaction between neighboring segments, ε, was set to -1.0 expressed in kT units. The calculations were performed on a 96 by 96 triangular lattice of equivalent adsorption sites at fixed temperature, T, and chemical potential of the adsorbate in the bulk phase, μ. For sufficiently low values of μ, our preliminary Monte Carlo modeling predicts the potential formation of two porous networks with very similar packing densities but markedly different symmetry. Figure 1c shows typical imperfect one-phase monolayer structures observed in the GCMC simulations in which the adsorbate density, ρ, was defined as the average number of segments per one lattice site. The packing, which consists of only one type of elongated honeycomb pores, where the longer chains form two parallel edges of the nanowells, belongs to the plane group *p*2 (Figure 1a). The packing with two types of pores, that is, a small honeycomb pore consisting of only shorter chains surrounded by larger triangular pores with alternating longer and shorter chains (which can be considered as a Kagomé network), belongs to the *p*6 plane group.

Increasing the chemical potential (adsorbate density) leads to the formation of a new molecular pattern involving close-packed linear structure of DBA1 molecules. Despite somewhat lower potential energy (see the Supporting Information, section A.1), the linear pattern is exceptionally stable at high adsorbate densities, as it offers closest packing of molecules of DBA1 on a triangular grid.

An important effect observed in the GCMC simulations is the formation of pure structures A and B within the same range of parameters, ρ and T, meaning that one of these structures is metastable. A simple argument for that is the Gibbs phase rule stating that three phases (*p*6, *p*2, and the 2D gas phase) cannot exist in a one-component system except from an isolated point on a $\rho-T$ plane. Although separate canonical

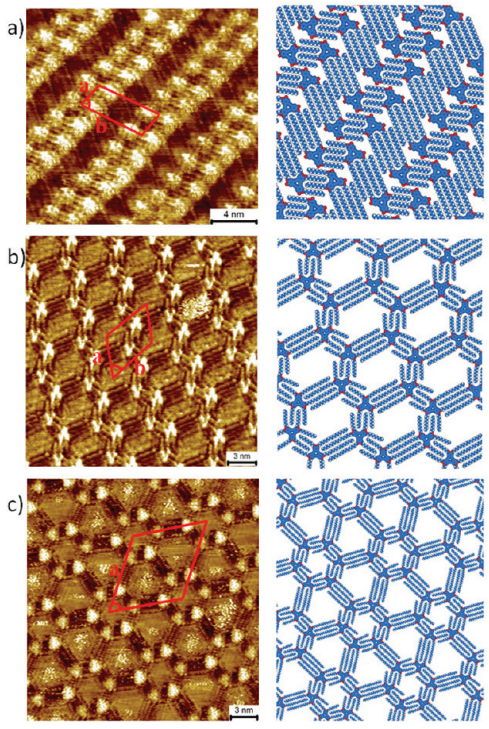

Figure 2. STM images of DBA1 at the TCB/HOPG interface and respective tentative molecular models in the (a) linear packing, where only the 2 OC_{20} and 2 OC_{10} chains are adsorbed, the remaining 2 OC_{10} chains which are not adsorbed are omitted for clarity (9.3×10^{-4} M, I_{set} = 0.1 nA, V_{set} = −0.8 V), (b) *p*2 symmetry packing (4.6×10^{-6} M, I_{set} = 0.1 nA, V_{set} = −0.2 V), and (c) *p*6 symmetry packing (4.6×10^{-6} M, I_{set} = 0.1 nA, V_{set} = −0.2 V). Unit cell parameters for the linear packing are as follows: *a* = 2.15 ± 0.06 nm, *b* = 5.82 ± 0.17 nm, α = 79 ± 2°; for the *p*2 symmetry packing, *a* = 3.96 ± 0.04 nm, *b* = 5.16 ± 0.08 nm, α = 63 ± 3°; and for the *p*6 symmetry packing, *a* = *b* = 8.22 ± 0.12 nm, α = 60 ± 1°.

MC calculations[31,32] performed at adsorbate densities $\rho \in \langle 0.4, 0.56 \rangle$ demonstrate the occurrence of both patterns, a detailed analysis of the phase equilibria in the adsorbed overlayer suggests (Figure S1 and Table S1) that the *p*6 structure is metastable with exceptionally long lifetime. Obviously, in real systems where solvent molecules are coadsorbed on the surface, this picture can change markedly as we are dealing with a two-component system in which the *p*2 and *p*6 structures can be stabilized or destabilized by the solvent molecules, and their presence is allowed through Gibbs phase rule. The simulated results suggest that in real situations the equilibrium between the porous patterns *p*6 and *p*2 at low and moderate adsorbate densities can be very sensitive to the chemical nature of the solvent used (size, shape, and functionality). On the other hand, one can expect that at high adsorbate densities (high solute concentrations) the solvent will not affect much the spontaneous organization of the molecules of DBA1 into the linear nonporous pattern.

Effect of Concentration and Solvent. In order to check the Monte Carlo predictions, DBA1 was dissolved in various solvents (typically ∼1 mg in 1 g of solvent), and these solutions were further diluted as indicated. After dilution to the desired concentration, a droplet of this solution was drop-casted on the basal plane of freshly cleaved graphite (HOPG). After self-assembly has set in (∼30 min), the monolayer was imaged with scanning tunneling microscopy (STM). During the first 30 min, disordered domains are observed next to fuzzy domains, while after 30 min, the monolayer is stabilized and no dynamics are observed. On the basis of the contrast in the STM images, the ordering of the molecules could easily be determined. The DBA cores turn up as bright (triangular) features, while the alkyl chains are the less bright lines connecting the DBA cores.[14,27]

As expected,[14,15] the self-assembly of DBA1 is influenced by the solute concentration. At a concentration of 9.3×10^{-4} M, DBA1 mainly forms a close-packed linear structure, similar to triangular DBAs, where the two longer OC_{20} chains and only two out of the four shorter OC_{10} chains are adsorbed and interdigitated on the surface in an alternating way (Figure 2a). At lower concentration (∼3×10^{-6} M) and in a various solvents, a mixture of the two porous packings (*p*2 and *p*6) is most often obtained. The unit cell parameters are independent of the solvent. In both porous packings, a fuzzy white feature is often observed inside the pores, which is attributed to mobile DBA1 molecules trapped inside the pores.

Similar to the DBAs containing six identical alkoxy chains, and other pore forming molecules, the formation of the nanowells is favored at lower solute concentrations. However, is there a preference for the *p*2 or *p*6 pattern, as predicted for solvent-free conditions using Monte Carlo simulations? In TCB, the solute concentration does not influence the ratio between *p*2 and *p*6 (Figures S4a and S5a): even at submonolayer (1.9×10^{-6} M) coverage, both *p*2 and *p*6 domains are found in the same ratio (69/31) (see Supporting Information, sections A.2 and A.3). Another trend was observed in 1-phenyloctane and 1-octanoic acid. While in 1-phenyloctane at high concentration (5.5×10^{-4} M), again the linear high-density packing is observed, at low concentration (2.8×10^{-6} M), a more or less equal occurrence of *p*2 and *p*6 is observed (48/52, Figure S4b). However, upon lowering the concentration even more to submonolayer conditions (6.9×10^{-7} M), *the p6 structure is formed exclusively in 1-phenyloctane* (Figure S5b). In 1-octanoic acid, at high concentration (5.9×10^{-4} M), again the high-density nonporous packing is observed dominantly, while at low concentration (3.0×10^{-6} M), the *p*2/*p*6 ratio is 94/6 (Figure S4c). Lowering the concentration to submonolayer conditions (9.9×10^{-7} M) leads to the *exclusive appearance of the p2 structure in 1-octanoic acid* (Figure S5c).

It can therefore be concluded that the appearance of porous and high-density phases is concentration-dependent, the porous ones being favored at the lower

TABLE 1. Summary of the Concentration Studies in the Different Solvents with the *p*2/*p*6 Ratios in Parentheses for the Low-Density Patterns

	concentration		
solvent	$\sim 5 \times 10^{-4}$ M	$\sim 3 \times 10^{-6}$ M	$\sim 1 \times 10^{-6}$ M
TCB	high density	low density (72/28)	low density (69/31)
1-phenyloctane	high density	low density (48/52)	low density (0/100)
1-octanoic acid	high density	low density (94/6)	low density (100/0)
1-phenyltetradecane	high density	low density (91/9)	low density (100/0)

concentrations. Moreover, despite the fact that they have nearly equal packing densities, the ratio of the *p*2 and *p*6 networks can also be influenced by the concentration and the choice of solvent. It is even possible to exclusively form one of both porous patterns. However, the specific role of the solvent remains uncertain, as the solvent molecules are too mobile to be visualized in our experiments. Our hypothesis is that long alkylated solvent molecules tend to stabilize the *p*2 structure more than the *p*6. For instance, in 1-octanoic acid, hydrogen-bonded dimers of 1-octanoic acid molecules could fit inside the pore of the *p*2 network and stabilize it through van der Waals interactions with the longer rims of the DBA1 pore (Figure S6). The observation that for a constant DBA1 concentration ($\sim 3 \times 10^{-6}$ M) increasing the alkyl chain length of the solvent (1-phenyloctane, 1-phenyldecane, 1-phenyldodecane, and 1-phenyltetradecane, Table S2) shifts the ratio of *p*2/*p*6 from 48/52 to 91/9 and is also in line with the hypothesis. Representative results are summarized in Table 1.

Effect of Temperature. Neglecting the role of solvent, both the *p*2 and *p*6 patterns should have very similar energies: they have nearly the same surface density, and the intermolecular interactions (*e.g.*, alkyl chain interdigitation interactions) and molecule−substrate interactions are virtually identical. The Monte Carlo simulations confirmed this and concluded that in the absence of solvent the *p*6 structure is a metastable phase, while the *p*2 phase is the thermodynamically stable structure. Therefore, we also probed the effect of temperature and annealing.

In TCB, DBA1 forms a porous packing consisting of the *p*2 and *p*6 structures in a 72/28 ratio at room temperature at a concentration of 4.6×10^{-6} M. Upon heating the sample to 30 °C, this ratio is changed to 83/17, and further heating to 40 and 50 °C resulted in a 100% appearance of the *p*2 structure. Cooling to room temperature (~30 min) did not change this situation: the *p*2 structure is still observed at a 100% appearance (Figure S7a). In 1-phenyloctane and 1-octanoic acid, another trend was observed. Upon increasing the temperature, the porous structure is completely transformed into the linear packing from 30 °C on in 1-phenyloctane (2.8×10^{-6} M, Figure S7b) and from

TABLE 2. Summary of Temperature Studies in the Three Solvents in a Liquid Cell

solvent (concentration)	25 °C	30 °C	40 °C	50 °C
TCB (4.6×10^{-6} M)	72/28[a]	83/17	100/0	100/0
1-phenyloctane (2.8×10^{-6} M)	48/52	NA[b]	NA	NA
1-octanoic Acid (3.0×10^{-6} M)	94/6	*p*2/NA	NA	NA

[a] The indicated ratios are *p*2/*p*6 ratios.. [b] NA refers to the formation of a high-density phase.

40 °C on in 1-octanoic acid (3.0×10^{-6} M, Figure S7c). Cooling to room temperature resulted again in no additional change in the network: the linear packing is observed homogenously. These experiments were repeated several times reproducibly at different cooling rates: both cooling slowly in steps of 5 °C every 30 min and cooling fast by switching off the heating plate resulted in the same outcome.

This tendency to go to the *p*2 structure in case of TCB can be understood in terms of thermodynamics. From the Monte Carlo simulations, the *p*6 network is a metastable phase with an exceptionally long lifetime, but in an initial stage, a mixture of both *p*2 and *p*6 is expected, where the *p*6 network is believed to be kinetically trapped.[20] This is in line with the experiments in TCB, where more *p*2 structures are formed at room temperature (72%). Increasing the temperature provides enough energy for molecules trapped in these metastable *p*6 arrangements to reorganize and therefore allows the network to evolve toward its thermodynamic minimum, assisted by the solvent. Increasing the temperature causes any remaining *p*6 structures to transform into *p*2 and indicates experimentally that in TCB as a solvent, the *p*2 structure is thermodynamically favored over the *p*6 structure. Regardless of the fact if the porous phase at room temperature in 1-phenyloctane or 1-octanoic acid is thermodynamically favored or not, the transition into the high-density phase can be rationalized by a reduction in the stability of the porous networks if, for instance, solvent molecules start to desorb from the pores upon heating, a phenomenon which is not proven so far though. However, solvent desorption is expected to occur prior to DBA1 desorption given the differences in their adsorption energy. This transition occurs because the linear packing has a higher adsorption energy per unit area due to its increased packing density. The idea of structural rearrangements induced by solvent desorption also helps to explain the difference in behavior between 1-phenyloctane and 1-octanoic acid. The carboxylic acid group present in 1-octanoic acid allows the formation of intermolecular hydrogen bonds, which provide increased stabilization in comparison to 1-phenyloctane. This increased stabilization leads to a slightly higher transition temperature for 1-octanoic acid. Upon cooling, the dense-packed network can be considered as kinetically trapped, due to the relatively large energy barrier between the

dense-packed and the porous networks. All results are summarized in Table 2. Despite the effect of temperature on the self-assembly of DBA1 is not completely understood, it can be used as a tool to selectively and homogenously induce a specific network. A more extensive study on the temperature effect on the self-assembly of triangular DBAs is ongoing.

Host–Guest Architectures. Apart from being relevant to the formation of the DBA1 porous network, the voids in these patterns are ideally suited for the selective trapping of small guest molecules. Self-assembly of DBA1 potentially leads to the formation of three nanopores, which differ in size and shape. As one can imagine, these pores could display different affinities toward various guests and a specific pore shape could be used to select or even filter a specific guest molecule. Here we illustrate the host capabilities of both *p*2 and *p*6 networks toward several guest molecules including nanographene (NG),[33] coronene (COR), and isophthalic acid (ISA)[34] (Chart 1). In order to probe the host properties of the *p*2 structure, conditions where DBA1 exclusively forms the *p*2 structure were selected, such as in 1-octanoic acid at low DBA1 concentration. Upon premixing COR (3.0×10^{-3} M) and ISA (5.5×10^{-3} M) with DBA1 (2.9×10^{-6} M), a disordered network is observed. COR_1–ISA_6 clusters (COR_1–ISA_6, Chart 1) can be found inside the cavities of both *p*2 and *p*6 structures. The formation of the latter one is stabilized by the addition of COR and ISA. Upon heating to 50 °C though, the network is completely transformed into the *p*2 structure and the COR_1–ISA_6 clusters can be found inside the cavities (inset Figure 3b). The pores of the *p*2 structure have a matching width but lack length complementarity, making the guest molecules mobile inside the pores, and usually, the adsorbed COR_1–ISA_6 cluster is accompanied by a fuzzy feature inside the pore. Molecular modeling suggests that apart from the COR_1–ISA_6 cluster up to two COR molecules can fit inside the *p*2 void, which accounts for the fuzzy features (Figure 3c). Note that, in absence of the guest molecules, the formation of a high-density phase is expected at this DBA1 concentration and temperature.

To comply to conditions where a *p*6 network is formed in the absence of guest molecules, and to take advantage of the fact that a *p*6 network can potentially host more guest(s) (complexes) because of its two types of cavities, the self-assembly of a mixture of DBA1 (6.9×10^{-7} M), COR (3.0×10^{-3} M), ISA (5.5×10^{-3} M), and NG (1.7×10^{-3} M) is probed at the 1-phenyloctane/graphite interface. The *p*6 structure is still mainly observed and the COR_1–ISA_6 cluster can be identified in the small hexagonal pore of the *p*6 structure. Moreover, three NG molecules reside in the larger pores. However, the domains of this four-component 2D pattern remain quite small, and frequently, domains of pure guest molecules are observed (pure NG or pure COR_1–ISA_6 domains, Figure S8 in Supporting Information). Heating the monolayer did not result in larger domains of the four-component structure.

Chart 1. Chemical structures of the three guest molecules: isophthalic acid (ISA), coronene (COR), and nanographene (NG) and a molecular model of the COR_1–ISA_6 cluster.

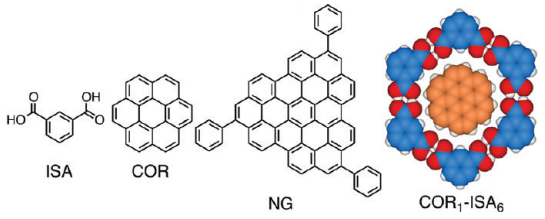

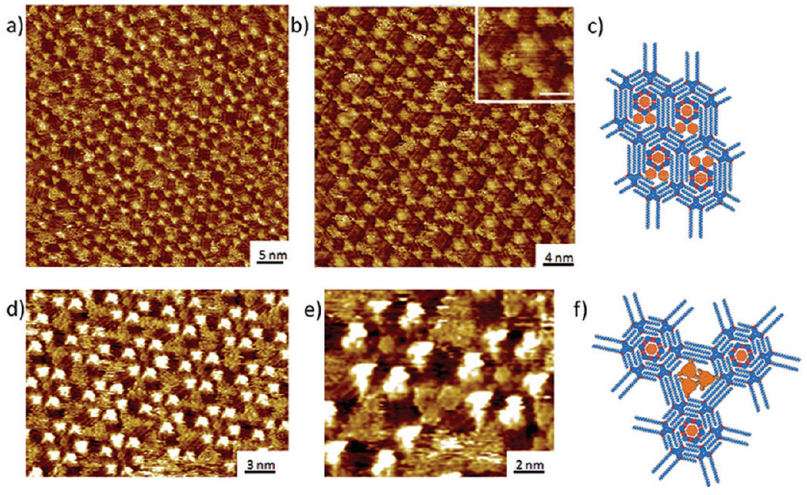

Figure 3. STM images of (a) a monolayer of DBA1 (2.9×10^{-6} M) mixed with COR (3.0×10^{-3} M) and ISA (5.5×10^{-3} M) at room temperature at the 1-octanoic acid/graphite interface, (b) the same monolayer of DBA1, COR, and ISA after annealing at 50 °C; the inset shows a zoom of the pore with the COR_1–ISA_6 cluster inside (scale bar is 1 nm). (c) Tentative corresponding models of DBA1 mixed with COR and ISA. (d,e) Monolayer of DBA1 (6.9×10^{-7} M), COR (3.0×10^{-3} M), ISA (5.5×10^{-3} M), and NG (1.7×10^{-3} M) at the 1-phenyloctane/graphite interface; the COR_1–ISA_6 cluster can be found immobilized in the small pore, while three NG molecules can be found in the larger pore. (f) Tentative corresponding model of the four-component structure.

So, both *p*2 and *p*6 structures have excellent host capabilities toward guest molecules with specific size and shape complementarity. Moreover, the presence of the guest molecules stabilizes the porous network and prevents it from collapsing under increased temperatures. Indeed, for the guest containing networks, no desorption of guest molecules was observed on raising the temperature. Note that in both cases sequential deposition of the molecular components yields similar results, but premixing gives rise to larger domain sizes and less phase separation.

CONCLUSION

We have shown that, by using DBA1 as building block, two different porous structures can be obtained, a *p*2 and a *p*6 pattern, which are nearly identical in packing density and only differ in symmetry. This result was predicted by Monte Carlo simulations and confirmed experimentally by probing the self-assembled monolayer with STM. The ratio of *p*2 and *p*6 structures can be influenced by controlling the concentration, solvent, temperature, and annealing history, leading under specific conditions to the formation of physisorbed monolayers belonging to the *p*2 or *p*6 plane group. The resulting nanoporous networks can be utilized as host networks to selectively trap a variety of guest molecules or guest complexes. In this way, it was even possible for three different guest molecules to be hosted at the same time in a spatially resolved way, leading to a surface-confined four-component supramolecular assembly. These results lead to a better understanding of self-assembly behavior of molecular building blocks into porous networks and show the importance of the interplay of various experimental parameters such as the choice of solvent, concentration, and temperature. Insight into the relative contribution of these factors will lead to a better control and pave the way for the future design of multicomponent and multifunctional self-assembled networks.

EXPERIMENTAL SECTION

The synthesis of DBA1 is described in section B of the Supporting Information. Nanographene (NG) was supplied from K. Müllen (MPI for Polymer Research, Mainz) and was synthesized following published protocols.[33] Commercially available 1-octanoic acid (Acros Co.), 1-phenyloctane (Acros Co.), 1,2,4-trichlorobenzene (Acros Co.), coronene (Aldrich Co.), and isophthalic acid (Acros Co.) were used as received. Solutions of DBA1 were prepared in commercially available 1-octanoic acid, 1-phenyloctane, and 1,2,4-trichlorobenzene (concentration range from 10^{-4}–10^{-7} M). These solutions were drop-casted on the basal plane of freshly cleaved highly oriented pyrolytic graphite (HOPG, grade ZYB, Advanced Ceramics Inc., Cleveland, OH). All images were taken in the constant current mode by using a Pico SPM (Agilent) with mechanically cut Pt/Ir (80/20) tips. By variation of the sample bias, the underlying graphite image was taken in order to correct for scanner drift by using scanning probe imaging processor (SPIP) software. Temperature experiments were done inside a liquid cell to avoid solvent evaporation linked with a temperature controller (Agilent).

Acknowledgment. This work is supported by K.U. Leuven through GOA, the Institute of Promotion of Innovation by Science and Technology in Flanders (I.W.T.), the Fund of Scientific Research Flanders (FWO), the Belgian Federal Science Policy Office through IAP-6/27, a Grant-in-aid for Scientific Research from the Ministry of Education, Culture, Sports, Science and Technology, Japan, and the National Science Foundation of China (21173061). We thank K. Müllen (MPI for Polymer Research, Mainz) for providing us with the nanographene molecule.

Supporting Information Available: Extra STM and Monte Carlo simulation results and details on the synthesis. This material is available free of charge *via* the Internet at http://pubs.acs.org.

REFERENCES AND NOTES

1. Ciesielski, A.; Palma, C. A.; Bonini, M.; Samori, P. Towards Supramolecular Engineering of Functional Nanomaterials: Pre-programming Multi-component 2D Self-Assembly at Solid–Liquid Interfaces. *Adv. Mater.* **2010**, *22*, 3506–3520.
2. Kudernac, T.; Lei, S. B.; Elemans, J.; De Feyter, S. Two-Dimensional Supramolecular Self-Assembly: Nanoporous Networks on Surfaces. *Chem. Soc. Rev.* **2009**, *38*, 402–421.
3. Elemans, J.; Lei, S. B.; De Feyter, S. Supramolecular Networks on Surfaces: From 2D Crystal Engineering to Reactivity. *Angew. Chem., Int. Ed.* **2009**, *48*, 7298–7332.
4. Bartels, L. Tailoring Molecular Layers at Metal Surfaces. *Nat. Chem.* **2010**, *2*, 87–95.
5. Barth, J. V. Molecular Architectonic on Metal Surfaces. *Annu. Rev. Phys. Chem.* **2007**, *58*, 375–407.
6. Nath, K. G.; Ivasenko, O.; MacLeod, J. M.; Miwa, J. A.; Wuest, J. D.; Nanci, A.; Perepichka, D. F.; Rosei, F. Crystal Engineering in Two Dimensions: An Approach to Molecular Nanopatterning. *J. Phys. Chem. C* **2007**, *111*, 16996–17007.
7. Bonifazi, D.; Mohnani, S.; Llanes-Pallas, A. Supramolecular Chemistry at Interfaces: Molecular Recognition on Nanopatterned Porous Surfaces. *Chem.—Eur. J.* **2009**, *15*, 7004–7025.
8. Theobald, J. A.; Oxtoby, N. S.; Phillips, M. A.; Champness, N. R.; Beton, P. H. Controlling Molecular Deposition and Layer Structure with Supramolecular Surface Assemblies. *Nature* **2003**, *424*, 1029–1031.
9. Stepanow, S.; Lingenfelder, M.; Dmitriev, A.; Spillmann, H.; Delvigne, E.; Lin, N.; Deng, X. B.; Cai, C. Z.; Barth, J. V.; Kern, K. Steering Molecular Organization and Host–Guest Interactions Using Two-Dimensional Nanoporous Coordination Systems. *Nat. Mater.* **2004**, *3*, 229–233.
10. Schull, G.; Douillard, L.; Fiorini-Debuisschert, C.; Charra, F.; Mathevet, F.; Kreher, D.; Attias, A. J. Single-Molecule Dynamics in a Self-Assembled 2D Molecular Sieve. *Nano Lett.* **2006**, *6*, 1360–1363.
11. Li, M.; Deng, K.; Lei, S. B.; Yang, Y. L.; Wang, T. S.; Shen, Y. T.; Wang, C. R.; Zeng, Q. D.; Wang, C. Site-Selective Fabrication of Two-Dimensional Fullerene Arrays by Using a Supramolecular Template at the Liquid–Solid Interface. *Angew. Chem., Int. Ed.* **2008**, *47*, 6717–6721.
12. Cardenas, L.; Lipton-Duffin, J.; Rosei, F. Transformations of Molecular Frameworks by Host–Guest Response: Novel Routes toward Two-Dimensional Self-Assembly at the Solid–Liquid Interface. *Jap. J. Appl. Phys.* **2011**, *50*, 08LA02–08LA02-6.
13. Kampschulte, L.; Werblowsky, T. L.; Kishore, R. S. K.; Schmittel, M.; Heckl, W. M.; Lackinger, M. Thermodynamical Equilibrium of Binary Supramolecular Networks at the Liquid–Solid Interface. *J. Am. Chem. Soc.* **2008**, *130*, 8502–8507.
14. Lei, S. B.; Tahara, K.; De Schryver, F. C.; Van der Auweraer, M.; Tobe, Y.; De Feyter, S. One Building Block, Two Different

Supramolecular Surface-Confined Patterns: Concentration in Control at the Solid–Liquid Interface. *Angew. Chem., Int. Ed.* **2008**, *47*, 2964–2968.
15. Tahara, K.; Okuhata, S.; Adisoejoso, J.; Lei, S.; Fujita, T.; De Feyter, S.; Tobe, Y. 2D Networks of Rhombic-Shaped Fused Dehydrobenzo[12]annulenes: Structural Variations under Concentration Control. *J. Am. Chem. Soc.* **2009**, *131*, 17583–17590.
16. Palma, C. A.; Bonini, M.; Llanes-Pallas, A.; Breiner, T.; Prato, M.; Bonifazi, D.; Samori, P. Pre-programmed Bicomponent Porous Networks at the Solid–Liquid Interface: The Low Concentration Regime. *Chem. Commun.* **2008**, 5289–5291.
17. Zhang, X.; Chen, T.; Chen, Q.; Deng, G. J.; Fan, Q. H.; Wan, L. J. One Solvent Induces a Series of Structural Transitions in Monodendron Molecular Self-Assembly from Lamellar to Quadrangular to Hexagonal. *Chem.—Eur. J.* **2009**, *15*, 9669–9673.
18. Ahn, S.; Matzger, A. J. Anatomy of One-Dimensional Cocrystals: Randomness into Order. *J. Am. Chem. Soc.* **2009**, *131*, 13826–13832.
19. Gutzler, R.; Sirtl, T.; Dienstmaier, J. F.; Mahata, K.; Heckl, W. M.; Schmittel, M.; Lackinger, M. Reversible Phase Transitions in Self-Assembled Monolayers at the Liquid–Solid Interface: Temperature-Controlled Opening and Closing of Nanopores. *J. Am. Chem. Soc.* **2010**, *132*, 5084–5090.
20. Bellec, A.; Arrigoni, C.; Schull, G.; Douillard, L.; Fiorini-Debuisschert, C.; Mathevet, F.; Kreher, D.; Attias, A. J.; Charra, F. Solution-Growth Kinetics and Thermodynamics of Nanoporous Self-Assembled Molecular Monolayers. *J. Chem. Phys.* **2011**, *134*, 124702–124708.
21. Marie, C.; Silly, F.; Tortech, L.; Müllen, K.; Fichou, D. Tuning the Packing Density of 2D Supramolecular Self-Assemblies at the Solid–Liquid Interface Using Variable Temperature. *ACS Nano* **2010**, *4*, 1288–1292.
22. Yang, Y.; Wang, C. Solvent Effects on Two-Dimensional Molecular Self-Assemblies Investigated by Using Scanning Tunneling Microscopy. *Curr. Opin. Colloid Interface Sci.* **2009**, *14*, 135–147.
23. Gutzler, R.; Lappe, S.; Mahata, K.; Schmittel, M.; Heckl, W. M.; Lackinger, M. Aromatic Interaction *vs*. Hydrogen Bonding in Self-Assembly at the Liquid–Solid Interface. *Chem. Commun.* **2009**, 680–682.
24. Li, Y.; Ma, Z.; Qi, G.; Yang, Y.; Zeng, Q.; Fan, X.; Wang, C.; Huang, W. Solvent Effects on Supramolecular Networks Formed by Racemic Star-Shaped Oligofluorene Studied by Scanning Tunneling Microscopy. *J. Phys. Chem. C* **2008**, *112*, 8649–8653.
25. Tahara, K.; Lei, S. B.; Adisoejoso, J.; De Feyter, S.; Tobe, Y. Supramolecular Surface-Confined Architectures Created by Self-Assembly of Triangular Phenylene–Ethynylene Macrocycles *via* van der Waals Interaction. *Chem. Commun.* **2010**, *46*, 8507–8525.
26. Lei, S. B.; Tahara, K.; Adisoejoso, J.; Balandina, T.; Tobe, Y.; De Feyter, S. Towards Two-Dimensional Nanoporous Networks: Crystal Engineering at the Solid–Liquid Interface. *CrystEngComm* **2010**, *12*, 3369–3381.
27. Tahara, K.; Furukawa, S.; Uji-I, H.; Uchino, T.; Ichikawa, T.; Zhang, J.; Mamdouh, W.; Sonoda, M.; De Schryver, F. C.; De Feyter, S.; *et al.* Two-Dimensional Porous Molecular Networks of Dehydrobenzo[12]annulene Derivatives *via* Alkyl Chain Interdigitation. *J. Am. Chem. Soc.* **2006**, *128*, 16613–16625.
28. Tahara, K.; Lei, S.; Mössinger, D.; Kozuma, H.; Inukai, K.; Van der Auweraer, M.; De Schryver, F. C.; Höger, S.; Tobe, Y.; De Feyter, S. Giant Molecular Spoked Wheels in Giant Voids: Two-Dimensional Molecular Self-Assembly Goes Big. *Chem. Commun.* **2008**, 3897–3899.
29. Lei, S.; Tahara, K.; Tobe, Y.; De Feyter, S. Role of Pseudopolymorphism on Concentration Dependent Competitive Adsorption at a Liquid/Solid Interface. *Chem. Commun.* **2010**, 9125–9127.
30. Lei, S.; Tahara, K.; Müllen, K.; Szabelski, P.; Tobe, Y.; De Feyter, S. Mixing Behavior of Alkoxylated Dehydrobenzo[12]annulenes at the Solid–Liquid Interface: Scanning Tunneling Microscopy and Monte Carlo Simulations. *ACS Nano* **2011**, *5*, 4145–4157.
31. Frenkel, D.; Smit, B. *Understanding Molecular Simulation*; Academic Press: London, 2002.
32. Szabelski, P.; De Feyter, S.; Drach, M.; Lei, S. B. Computer Simulation of Chiral Nanoporous Networks on Solid Surfaces. *Langmuir* **2010**, *26*, 9506–9515.
33. Feng, X. L.; Wu, J. S.; Ai, M.; Pisula, W.; Zhi, L. J.; Rabe, J. P.; Müllen, K. Triangle-Shaped Polycyclic Aromatic Hydrocarbons. *Angew. Chem., Int. Ed.* **2007**, *46*, 3033–3036.
34. Adisoejoso, J.; Tahara, K.; Okuhata, S.; Lei, S.; Tobe, Y.; De Feyter, S. Two-Dimensional Crystal Engineering: A Four-Component Architecture at a Liquid–Solid Interface. *Angew. Chem., Int. Ed.* **2009**, *48*, 7353–7357.